7-1-2016

MEASUREMENT OF THERMAL PROPERTIES AND POROSITY OF CONSOLIDATED SALT.

Laxmi Prasad Paneru

Laxmi Prasad Paneru
Candidate

Civil Engineering
Department

This thesis is approved, and it is acceptable in quality and form for publication:

Approved by the Thesis Committee:

Dr. John C. Stormont, Chairperson

Dr. Tang-Tat Ng, Member

Dr. Stephen J. Bauer, Member

MEASUREMENT OF THERMAL PROPERTIES AND POROSITY OF CONSOLIDATED SALT

by

LAXMI PRASAD PANERU

THESIS

Submitted in Partial Fulfillment of the
Requirements for the Degree of

Master of Science
Civil Engineering

The University of New Mexico
Albuquerque, New Mexico

July 2016

ACKNOWLEDGEMENTS

First, I would like to extend my sincere gratitude to my advisor, Dr. John C. Stormont for providing me the opportunity of studying master's degree in Civil Engineering. His valuable guidance, motivation and patience made this thesis possible. I would like to thank Dr. Tang-Tat Ng for his valuable time and accepting my request for being in my thesis examination committee. I would like to especially thank committee member Dr. Steven J. Bauer for providing me an access to Sandia National Laboratories, where most of the experiments were done.

I would like to acknowledge the United States Department of Energy, Nuclear Energy University Program for the project funding. I would like to express my thankfulness to my project group members: Brandon Lampe, Melissa Mills, Timothy Lynn, and Aayush Piya.

MEASUREMENT OF THERMAL PROPERTIES AND POROSITY OF CONSOLIDATED SALT

by Laxmi Prasad Paneru

B.Sc. Civil Engineering, Tribhuvan University, 2010
M.S. Civil Engineering, University of New Mexico, 2016

ABSTRACT

Salt formations may be used as repositories for long term isolation of nuclear waste. Excavating drifts in a subsurface salt formation produces granular salt spoils, which could be used as sealing material for boreholes and drifts. In drifts, the backfilled salt would conduct heat from the waste load to the host rock salt. The efficiency of heat dissipated from the backfill will depend on the thermal properties of the backfill. The results of this study show how these thermal properties evolve with the porosity of consolidating granular salt.

Thermal properties and porosity of laboratory-consolidated salt and in situ partially consolidated salt were determined. The laboratory-consolidated salt was consolidated under a range of hydrostatic stresses with temperature and moisture conditions relevant to a potential repository environment. Additional measurements were made on an intact salt crystal and dilated polycrystalline host rock salt from the WIPP facility. Thermal properties in this study were measured using a transient plane source method at temperatures ranging from 50 ˚C to 250 ˚C.

Porosity and grain density were measured using a porosimeter; granular salt porosities ranged from 0.005 to 0.33, with an average grain density of 2.161 g/cc. Thermal conductivity of granular salt was shown to be dependent on temperature as well as porosity; thermal conductivities decreased with increase in temperature and porosity. Thermal conductivity of dilated salt was lower than

consolidated salt at comparable porosities. This is believed to be caused by the pervasive crack network present in the dilated salt which is expected to inhibit flow of heat more than the pores present in the consolidated salt. Specific heat of granular salt at lower temperatures decreased with increasing in porosity. At higher temperatures, porosity dependence was not apparent.

The thermal conductivity and specific heat data were fit to empirical models and compared with results presented in literature. At comparable densities, the thermal conductivities of granular salt samples consolidated hydrostatically in this study were greater than those measured previously on samples formed by quasi-static pressing. Photomicrographs of thin sections suggested that the method of consolidation influenced the nature of the porosity of the samples (e.g., crack vs. pore), and this may account for the variation of measured thermal conductivities between the two consolidation methods.

TABLE OF CONTENTS

LIST OF FIGURES

LIST OF TABLES

Chapter 1 INTRODUCTION

1.1 BACKGROUND

The nation's decades of commercial nuclear power production and nuclear weapons production have resulted in a growing inventory of spent nuclear fuel and other high-level nuclear wastes that are being temporarily stored [1]. The long-term goal of the US government is to permanently dispose of these wastes in an appropriate facility; underground repositories are a leading candidate for providing long-term radioactive waste isolation. Salt formations have several favorable attributes for this application [2, 3, 4]. The existence of massive, stable salt formations and their low permeability and porosity characteristics, indicates they are effectively isolated from groundwater. Salt creeps plastically, which results in the closure of shafts and tunnels in salt eventually entombing the waste. Salt is also an excellent conductor of heat and will tend to dissipate heat generated from the waste. Salt formations are being used as a medium for some radioactive waste disposal. In the USA, the Waste Isolation Pilot Plant (WIPP), constructed in a bedded salt formation in Southeastern New Mexico, is storing defense-generated transuranic wastes. In Germany, radioactive wastes have been stored in mines developed in domal salt formations that were converted to radioactive waste storage facilities.

Granular salt, a by-product of excavation, can be used as backfill material in drifts and shafts of a storage facility. Creep closure of formation surrounding the excavation exerts pressure on the granular salt and consolidates it into a density comparable to intact salt. The time-dependent consolidation of granular salt can reduce its porosity from 0.4 in a loose state to an eventual end state of less than 0.01. Granular salt backfill will conduct heat away from the waste to the host rock as well as distribute the compressive load of surrounding formation onto the waste canisters

[3]. Elevated temperatures in the vicinity of heat generating waste will increase consolidation rates [5]. Owing to the dramatic impact that water has on accelerating consolidation [5, 6], a small amount of water will likely be added to granular salt as it is emplaced.

Because thermal properties of granular materials are a function of their porosity, moisture content, mineralogy, texture, and temperature, the thermal properties of granular salt are expected to change during consolidation. Porosity has a substantial effect on the thermal conductivity, with the magnitude of effect dependent on the arrangement of the pore space [2]. An understanding of how thermal properties change during consolidation is necessary to predict how a repository will respond to the heat generated from a radioactive waste load.

Thermal properties of salt crystals are known to be a function of temperature [7, 8, 9, 10, 11]. For example, Urquhart and Bauer [11] report the thermal conductivity of salt crystals decreased with increasing temperature, varying from 9.975 W/m K at -75 ˚C to 2.699 W/m K at 300 ˚C. For polycrystalline salt, thermal properties have been found to be a function of composition of impurities [2, 9, 10, 12], grain size [3], porosity [13], as well as temperature.

Bauer and Urquhart [13] measured thermal properties on granular salt at various porosities. They compressed granular salt from the WIPP into 50 mm diameter and 25 mm high pellets. The porosity of the samples was calculated as a ratio of bulk density of the pellet to the measured density of crushed salt (2.14 g/cc). Porosity of the samples ranged from 0.02 to 0.4. They also produced samples from commercially available cored salt licks formed by microcrystalline “solar salt.” More than 2000 thermal property measurements were made using guarded heat flow and

transient plane source methods. The thermal conductivity of granular salt showed strong temperature dependence: thermal conductivity decreased with increasing temperature and porosity [3]. Specific heat of granular salt increased with increasing temperature, but showed little porosity dependence. They compared their thermal conductivity results to that predicted from the geometric mean of the thermal conductivity of the sample constituents, sometimes referred to as the mixing law model that has been used to estimate thermal conductivity of other geologic materials [14]:

$$K_{gs} = K_{int}^{1-\phi} K_a^{\phi} \quad (1)$$

where ϕ is porosity, K_{gs} is thermal conductivity of granular salt, K_{int} is thermal conductivity of an intact salt crystal and K_a is thermal conductivity of air. They found that the measured thermal conductivities were lower than that predicted by Equation 1 in most cases. Bauer and Urquhart [13] also measured thermal properties of polycrystalline salt cores obtained from the WIPP facility. They found that the small porosities (0.02 to 0.04) in dilated polycrystalline salt have a greater effect on the thermal properties than comparable porosities in compressed granular salt. They suggested this result was due to the difference in the pore structure in the two materials: dilated polycrystalline salt tends to develop extensive and well-connected pore networks along grain boundaries whereas compressed salt may have more isolated pores.

Bechthold et al. [3, 15] report thermal properties of granular salt as part of an integrated program of the evaluation of domal salt formations in Germany for radioactive waste repositories. Granular salt obtained during the excavation of test drifts was sieved to obtain grain sizes less than 45 mm. The granular salt was re-emplaced in the test drifts. From the volume of emplaced granular salt and the total test drift volume, an initial backfill porosity of 0.35 was determined, corresponding to an initial density of 1.4 g/cc. Drift closure measurements were used to calculate the porosity of

consolidating backfill. Laboratory backfill compaction tests were performed in a triaxial cell at elevated temperatures and pressures on granular salt obtained from the excavation work. The grain size of salt ranged between 50 mm and 300 mm, and the highest temperature and pressure of the test was 200 ˚C and 70 MPa, respectively. A constant axial strain rate of about 10^{-5} s^{-1} was used for compaction and volume change was measured by a special pressure/volume controller device. Grain density of salt was determined using a pycnometer and bulk density was determined from the mass and volume of the salt used in the specimen. Porosity was calculated by:

$$\phi = 1 - \frac{\rho_B}{\rho_G} \quad (2)$$

where ρ_B is bulk density (g/cc) and ρ_G is salt grain density (g/cc). Thermal properties of the compacted salt was determined using a transient method in a porosity range of 0.013 to 0.285. Most of the tests were carried out at room temperature and a few experiments were carried out at 80 ˚C. Their initial results [3] suggested a linear relationship between thermal conductivity and porosity:

$$K_{gs} = K_{int}(1-2.7\phi) \quad (3)$$

Similarly, a linear relationship between specific heat of granular salt and porosity was recommended as:

$$C_{gs} = (1-\phi) C_{int} \quad (4)$$

where C_{gs} is specific heat of granular salt and C_{int} is the specific heat of intact salt crystal. They reported additional measurements [15] and indicated a polynomial best fit to data of thermal conductivity and porosity:

$$K_{gs} = K_{int}(-54\phi^4+74\phi^3-27.2\phi^2+0.3\phi+1) \quad (5)$$

1.2 OBJECTIVES

In this study, measurements of thermal properties, grain density, and porosity are reported for granular salt that has been hydrostatically consolidated under a range of temperature, stress, and moisture conditions. Additional tests were conducted on a single intact salt crystal and dilated polycrystalline salt. The objectives of this study are:

1. Determine thermal properties of granular salt consolidated to varying porosities as a function of temperature.
2. Use experimental results to develop expressions for changes in thermal properties with temperature and porosity.
3. Evaluate whether water added to granular salt samples prior to consolidation affects thermal properties.
4. Determine if the method of consolidation (hydrostatic creep consolidation) affects resulting thermal properties in consolidated granular salt by comparing these results with those obtained previously by others on samples that were formed by rapid pressing at ambient temperature.
5. Compare and contrast thermal properties obtained on dilated polycrystalline salt with granular salt at similar porosities.

Chapter 2 MATERIALS AND EXPERIMENTAL METHODOLOGY

2.1 SAMPLE MATERIAL

Thermal property and porosity measurements were made on four different sample groups: laboratory-consolidated granular salt using two salt types (domal and bedded), granular salt partially consolidated in situ recovered from an underground research facility, polycrystalline salt cores, and an intact halite crystal. The domal salt was obtained from Avery Island, LA (AI) and the bedded salt was from the WIPP facility. Thermal tests were conducted on 20 samples obtained from these salt types; many of these samples were subsequently cored to produce a total of 55 sub-samples used for porosity testing. A summary of samples and sub-samples is given in Table 1.

Table 1 Samples and sub-samples produced for thermal properties and porosity tests.

	Laboratory consolidated salt		In situ partially consolidated salt	Polycrystalline salt	Intact salt crystal
	WIPP	AI			
Samples	12	2	3	2	1
Sub-samples	36	8	6	5	

2.1.1 Laboratory-consolidated granular salt samples

The laboratory-consolidated granular salt specimens were consolidated by means of hydrostatic creep tests. Mine-run granular salt obtained from the WIPP facility and the Avery Island (AI) mine was sieved to obtain particle sizes of less than 9.5 mm. A representative grain size distribution of each salt type is given in Figure 1. The sieved granular salt was oven dried for 24 hours at 50 ˚C before compacting inside a jacket of lead and copper to withstand testing at elevated temperatures. Some specimens had 1% moisture by weight added prior to specimen construction. The resulting

cylindrical specimens were 100 mm in diameter, with a nominal height of 200 mm. The initial porosity of the specimens ranged from 0.34 to 0.4.

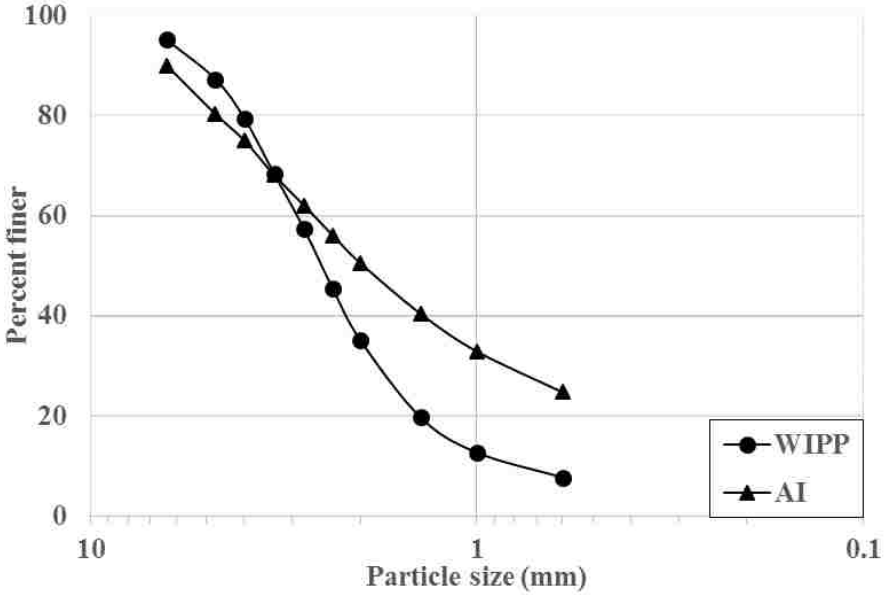

Figure 1 Grain size distribution of granular salt.

Specimens were consolidated using hydrostatic stresses up to 38 MPa and temperatures up to 250 ˚C. Stress and strain were derived from measured loads and deformations. In some tests, gas flow through the specimen during consolidation was measured. Test durations ranged from hours to weeks and most specimens achieved a final porosity of 0.05 or less. More details regarding the consolidation tests are given by Broome et al. [16].

After a consolidation test was completed, two discs, each approximately 25 mm thick, were cut from the top and bottom of the consolidated specimen using a diamond wire saw. The discs were used for thermal properties testing. Subsequently, one of the discs was further cored to obtain 25.4 mm and 38 mm diameter sub-samples for porosity measurements. These sub-samples were further cut to an approximate height of 12.7 mm and 25.4 mm (Figure 2).

Figure 2 A 25.4 mm diameter core obtained from 100 mm in diameter and 25 mm thick disc.

2.1.2 In situ partially consolidated granular salt

Cores of partially consolidated granular salt backfill were obtained from the BAMBUS (Backfill and Material Behavior in Underground Salt Repositories) project site within the Asse salt mine located in Germany. The backfill was pneumatically stowed in 1985 as part of a heater test initiated in 1990 and terminated in 1999. The backfill had consolidated to a porosity of 0.23 in the heated region and to 0.3 in the non-heated region when cores were obtained and tested in 1999 [3]. In August 2015, additional cores of this backfill were obtained. The diameter of the cores ranged from 83 mm to 100 mm. These cores were cut with a wire saw to obtain two discs, each of approximately 25 mm thickness. One of the discs was cored to obtain 25.4 mm diameter sub-samples. These sub-samples were further cut to an approximate height of 12.7 mm.

2.1.3 Dilated polycrystalline salt

Two 100 mm diameter cylindrical cores of polycrystalline salt were obtained from the WIPP facility. These cores had been previously subjected to uniaxial compression testing, one at 200 ˚C

and one at 250 ˚C, which caused dilation. The cores were subsequently cut along their vertical axis and tested for thermal properties at four different locations on the cut plane by Bauer and Urquhart [13]. For this study one of the cut halves was further cut along the horizontal and vertical axes to measure thermal conductivity in both the planes. Also, 25.4 mm diameter sub-samples with heights of 12.7 mm and 25.4 mm were obtained to test for porosity.

2.1.4 Intact salt crystal

A single crystal of optically clear halite was obtained from the Hockley Salt Dome in Texas. The crystal had a width of 75 mm and a height of 50 mm [11]. The crystal was assumed to have zero porosity.

2.2 EXPERIMENTAL METHODOLOGY

2.2.1 Porosity measurement

Porosity measurements were made on sub-samples using a helium gas expansion porosimeter. The apparatus consisted of a known reference volume (R) and a known sample cell volume (C) separated on either side by a valve (V_2) as shown in Figure 3. The sample cell was initially filled with standard billets of known volume. A sub sample of unknown grain volume G was placed inside the sample cell to replace a billet of volume B. Initial gas pressure of P_o was supplied at the upstream and isolated inside the reference volume. After equilibrium, V_2 was opened and gas was allowed to pass in the sample cell until a final equilibrium pressure P was achieved. Grain volume (G) was calculated using Coberly-Stevens equation [17].

$$G = R + C - R\frac{P_o}{P} \quad (6)$$

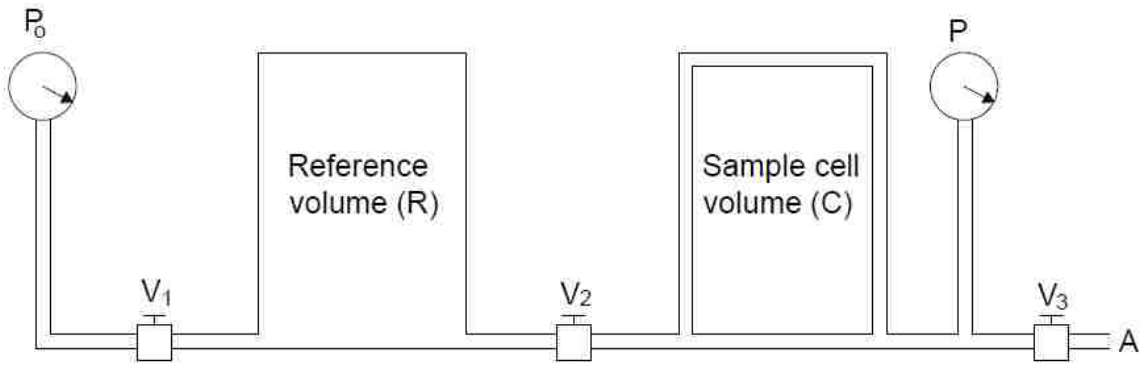

Figure 3 Schematic of a gas expansion porosimeter.

The sample cell was calibrated under two different conditions: first with all the billets inside the sample cell and second with a billet of volume B removed. The calibration equation derived using Equation 6 is:

$$R = \frac{B}{\frac{P_{ob}}{P_b} - \frac{P_{of}}{P_f}} \quad (7)$$

where P_{of} and P_f are initial and final pressures during the first calibration, and P_{ob} and P_b are initial and final pressures during the second calibration. The grain volume of tested sub-samples was determined by:

$$G = B + \frac{P_{of}}{P_f}R - \frac{P_{os}}{P_s}R \quad (8)$$

where P_{os} and P_s are initial and final pressures during the actual porosity test. Measurement of diameter and height were made at 4 different locations on the sub-sample using calipers. Volume and hence bulk density was calculated from dimension averages and the measured mass. Grain density was calculated from the measured grain volume (Equation 7) and mass. Finally, porosity was calculated using Equation 2.

The 25.4 mm and 38 mm diameter sub-samples had an approximate height of 12.7 mm or 25.4 mm; the volume of the sub-samples ranged from 6.08 cc to 14.87 cc. Porosity was also determined from the sub-sample dimensions and mass, referred to as the mass volume (MV) method. This method assumed a grain density of 2.16 g/cc for granular salt [7, 18] and utilized Equation 2 to calculate porosity. Based on independently measuring a sub-sample dimensions 23 times, the standard deviation in the sub-sample volume measurement was 0.01 cc.

The porosity of the central core from consolidated specimens was measured in a differential pressure permeameter that served as a gas expansion porosimeter. During the conduct of permeability tests on the central core, an initial pore pressure in the sample was established by introducing gas to the sample from a reservoir of known volume and pressure. The subsequent equilibrium pressure was used to estimate the connected pore volume (V_{pore}) in the sample:

$$V_{pore} = V_1(P_{eq}-P_1)/P_{eq} \quad (9)$$

where V_1 is the known volume of the permeameter, P_1 is the initial pressure in the permeameter, and P_{eq} is the equilibrium pressure after the sample is exposed to the permeameter.

2.2.2 Thermal properties measurement

Thermal properties measurements were made using the transient plane source method with a Hot Disk® TPS 1500. For this method, a heat pulse was applied with a thin plane sensor that was sandwiched between two pieces of consolidated salt. Thermal properties were interpreted numerically from the dissipation of the heat pulse with time.

Two discs of salt, with a diameter and thickness greater than the radius of the sensor were used, as recommended by the manufacturer. These discs were polished on one side to get a smooth and clean surface using fine sand paper and isopropanol. The thermal sensor was then pressed between the two polished sides and modest pressure was applied across the discs using a screw (Figure 4). A heat pulse was supplied and the transient temperature response was recorded for 20 to 40 seconds. A computer program integrated into the measurement system solved the transient heat equation for the thermal properties that best fit the measured temperature response. This solution assumes the thermal properties are uniform throughout the sample and thus averages out any local porosity and grain size heterogeneities [13]. Heat energy was dissipated by waiting 20 minutes between measurements. Heating power, test duration, and interval between successive measurements were automatically adjusted by the device to optimize the test conditions. Measurements were made at temperatures up to the maximum temperature during the consolidation testing or the uniaxial compression testing in the case of the dilated polycrystalline salt tests. In situ consolidated samples were tested up to 150 ˚C. Typically, three to five sets of measurements at each temperature were made at the same location and averaged; each set of measurements consisted of 5 individual measurements.

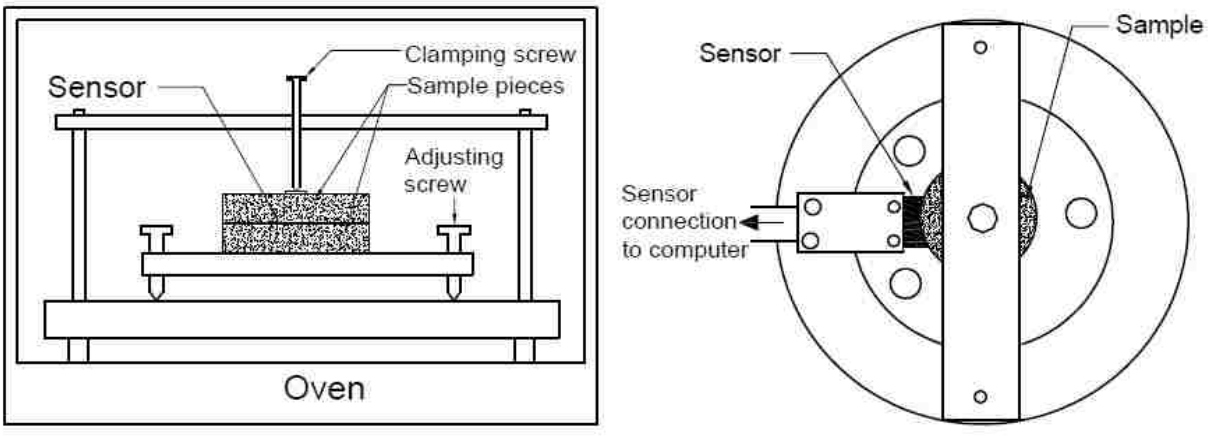

Figure 4 Schematic of thermal properties test arrangement shown in plan (right) and elevation (left).

Thermal tests were repeated on a consolidated salt sample 10 separate times to evaluate repeatability of the measurement. In each test, the sample was removed from test device and the sensor was repositioned in a different location before the next test was conducted. The standard deviation in thermal conductivity and specific heat at 50 ˚C estimated from the repeated measurements were 0.237 W/mK and 0.114 MJ/m^{3}K, respectively.

2.2.3 Microscopic observations

Microscopic observations were made on sections made from hydrostatically consolidated salt samples and some pellet compressed samples from the tests of Bauer and Urquhart [13] with comparable densities. Hydrostatically consolidated samples were vacuum impregnated with low viscosity epoxy that was doped with Rhodamine-B and cut with an Isomet® saw on a thin section chuck. The cut pieces were polished with a 1200 grit sandpaper to until they had 1 mm thickness. A Leitz Ortholux II optical microscope equipped with a Leica camera and Leica Application Suite software was used for microscopic observations. The pellet samples' thin sections were commercially prepared in a similar manner. Photomicrographs of both the salt types were taken at 5x magnification of the objective.

Chapter 3 RESULTS

3.1 POROSITY RESULTS

Porosity and grain density of all salt types are summarized in Table 2. Porosity of sub-samples ranged between 0.005 and 0.33. The average grain density of granular salt using WIPP and AI salt obtained from the porosimeter method performed on 58 unique tests was 2.161 g/cc with a standard deviation of ±0.009 g/cc. Grain density of BAMBUS samples determined from the porosimeter was comparatively greater than the other salt types; however it was consistent with the value of 2.187 g/cc reported by Bechthold et al. for salt from the Asse facility [3].

Table 2 Summary of porosity test.

Types of salt	Sample ID	Grain density from porosimeter (g/cc)	Sub-sample porosity		Porosity of central core
			Porosimeter	MV	
Laboratory consolidated salt	WP-HY-90-01	2.158	0.122	0.123	0.048
	WP-HY-90-02	2.160	0.035	0.036	0.015
	WP-HY-90-03	2.171	0.221	0.217	
	WP-HY-90-04	2.163	0.043	0.042	0.030
	WP-HY-90-07	2.163	0.019	0.017	0.014
	WP-HY-90-08	2.158	0.057	0.058	0.019
	WP-HY-90-09	2.170	0.328	0.253	
	WP-HY-175-01	2.150	0.062	0.066	0.047
	WP-HY-175-03	2.157	0.049	0.050	0.023
	WP-HY-175-04	2.164	0.045	0.043	0.022
	WP-HY-250-01	2.142	0.005	0.014	0.012
	WP-HY-250-02	2.167	0.018	0.014	
	AI-HY-250-01	2.164	0.027	0.025	
	AI-HY-250-02	2.161	0.012	0.011	
Polycrystalline salt	WP-DL-200	2.161	0.022	0.021	
	WP-DL-250	2.181	0.032	0.026	
In situ consolidated salt	BAMBUS-1-1.82	2.192	0.252	0.249	
	BAMBUS-1-2.77	2.181	0.209	0.211	
	BAMBUS-2	2.191	0.262	0.260	

Porosity of laboratory-consolidated samples determined from the porosimeter and MV methods were very close to one another (Figure 5). Similarly, the porosity of dilated and BAMBUS salt samples obtained from these methods were almost equal. Porosity of sub-samples measured with the porosimeter was greater than the porosity of central cores measured using the permeameter i.e., the porosity of end pieces is greater than that of the central core (Figure 5).

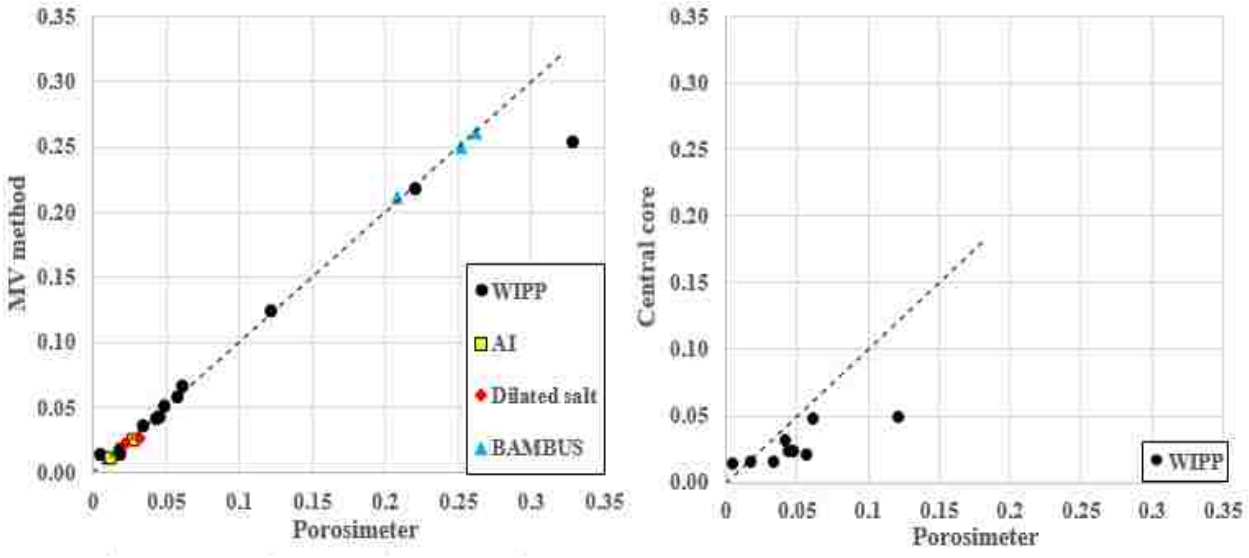

Figure 5 Comparison of porosities obtained from: porosimeter method and MV method (left), and porosimeter method and permeameter method (right).

To investigate the porosity variability within a parent sample of laboratory-consolidated salt, two discs were cored to produce 5 sub-samples each. The sub-samples were cored approximately equidistant from center to center of the individual cores and the center of the disc for maximum utilization of the material (Figure 6). All values fall within ±0.005 of the mean porosity values.

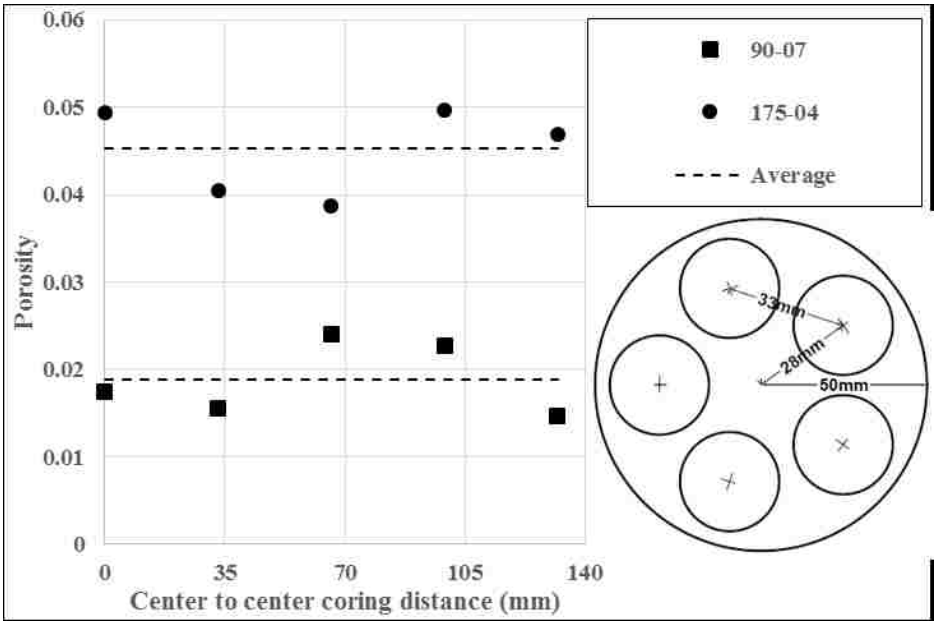

Figure 6 Radial variability of porosity in laboratory-consolidated samples.

3.2 THERMAL PROPERTIES RESULTS

Thermal conductivity and specific heat of an intact salt crystal, laboratory-consolidated salt, and in situ consolidated salt at various temperatures are given in Table 3 and plotted versus porosity in Figure 7. The intact salt data is given at zero porosity. Results indicate that thermal conductivity of intact salt crystal decreases with increase in temperature, while specific heat increases with increase in temperature. For granular salt, thermal conductivity decreases with increase in temperature and porosity. Specific heat increases with increase in temperature at lower porosities. At higher porosities temperature dependence is not apparent. At lower temperatures, specific heat decreases with increase in porosity. At higher temperatures porosity dependence is not apparent.

Table 3 Thermal properties of various salt types measured in a range of 50 ˚C to 250 ˚C.

Types of salt	Sample	Thermal conductivity (W/mK)					Specific heat (MJ/m^{3}K)				
		50˚C	100˚C	150˚C	200˚C	250˚C	50˚C	100˚C	150˚C	200˚C	250˚C
Laboratory-consolidated salt	WP-HY-90-01	4.30					2.15				
	WP-HY-90-02	5.44					1.20				
	WP-HY-90-03	2.70					1.99				
	WP-HY-90-04	4.81					2.02				
	WP-HY-90-07	5.09					1.74				
	WP-HY-90-08	4.75					1.70				
	WP-HY-90-09	1.85					0.56				
	WP-HY-175-01	4.10	3.37	2.87			1.91	1.87	1.88		
	WP-HY-175-03	4.38	4.07	3.78			1.85	2.04	2.19		
	WP-HY-175-04	4.40	4.08	3.74			2.03	2.18	2.33		
	WP-HY-250-01	5.02	4.73	4.32	3.86	3.53	1.97	2.21	2.42	2.47	2.62
	WP-HY-250-02	5.19	4.72	4.31	3.84	3.50	2.01	2.21	2.46	2.61	2.70
	AI-HY-250-01	5.38	4.94	4.54	4.13	3.76	1.96	2.17	2.39	2.53	2.64
	AI-HY-250-02	5.45	5.11	4.67	4.28	3.89	2.07	2.21	2.39	2.52	2.58
In situ consolidated salt	BAMBUS-1-1.82	2.15	1.97	1.61			1.27	1.42	1.37		
	BAMBUS-1-2.77	2.48	2.25	1.83			1.41	1.53	1.45		
	BAMBUS-2	2.20	2.01	1.68			1.06	1.27	1.26		
Intact crystal	INT-01	5.55	5.05	4.56	4.31	3.92	2.06	2.15	2.38	2.48	2.63

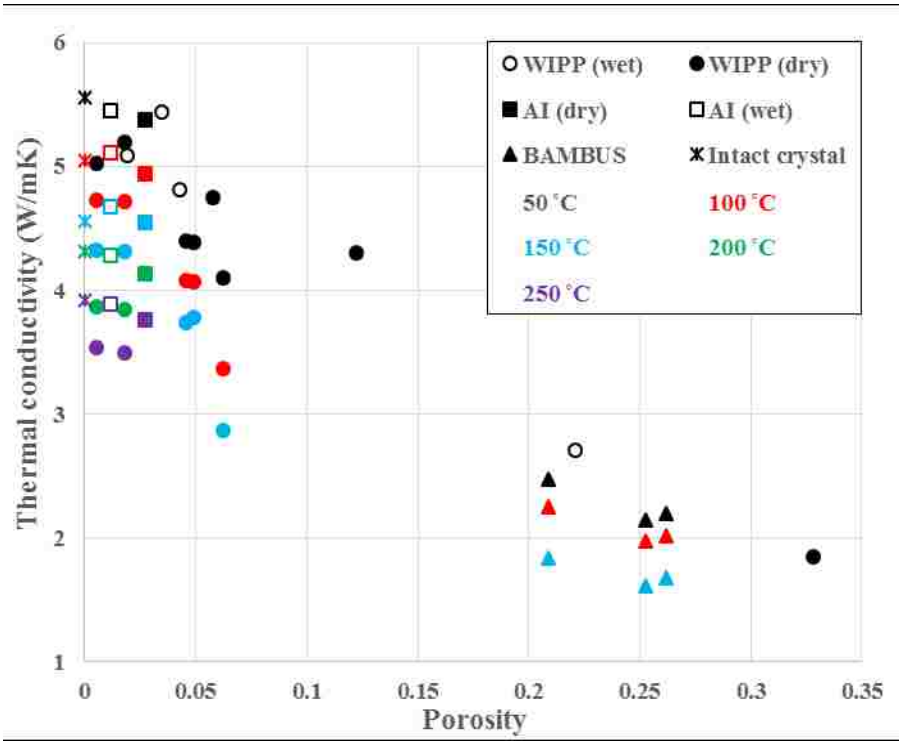

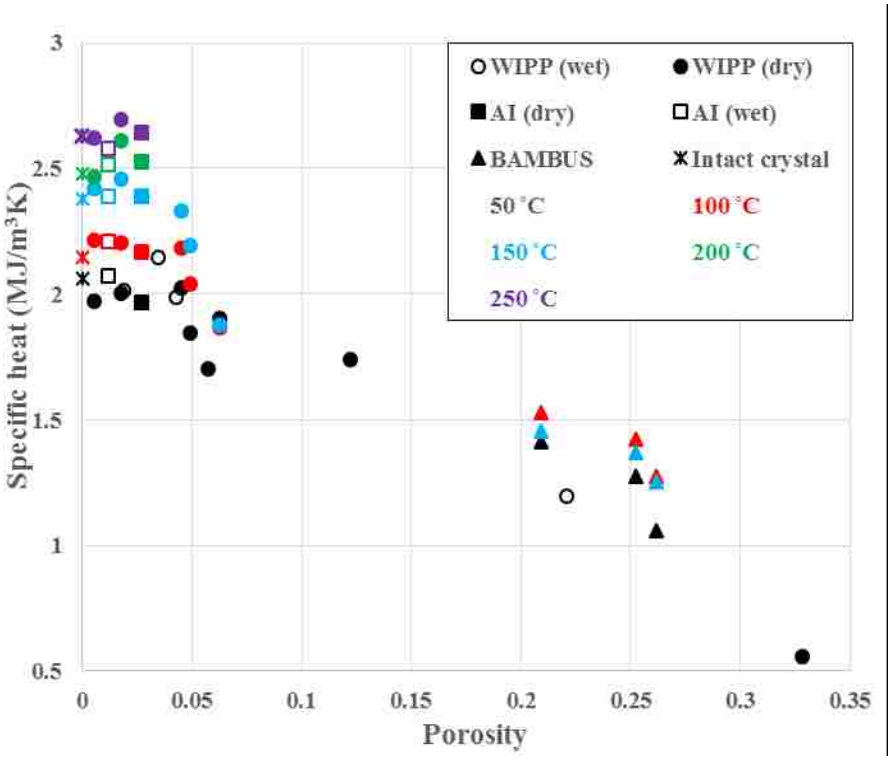

Figure 7 Thermal properties of sub-samples vs porosity at various temperatures.

Thermal conductivities of the dilated salt samples are given in Figure 8. For each sample, separate measurements were made in the vertical and horizontal plane. In one sample, the vertical and horizontal measurements nearly coincide, whereas in the other sample the values along the horizontal plane are larger. In all cases, the thermal conductivity decreased with temperature.

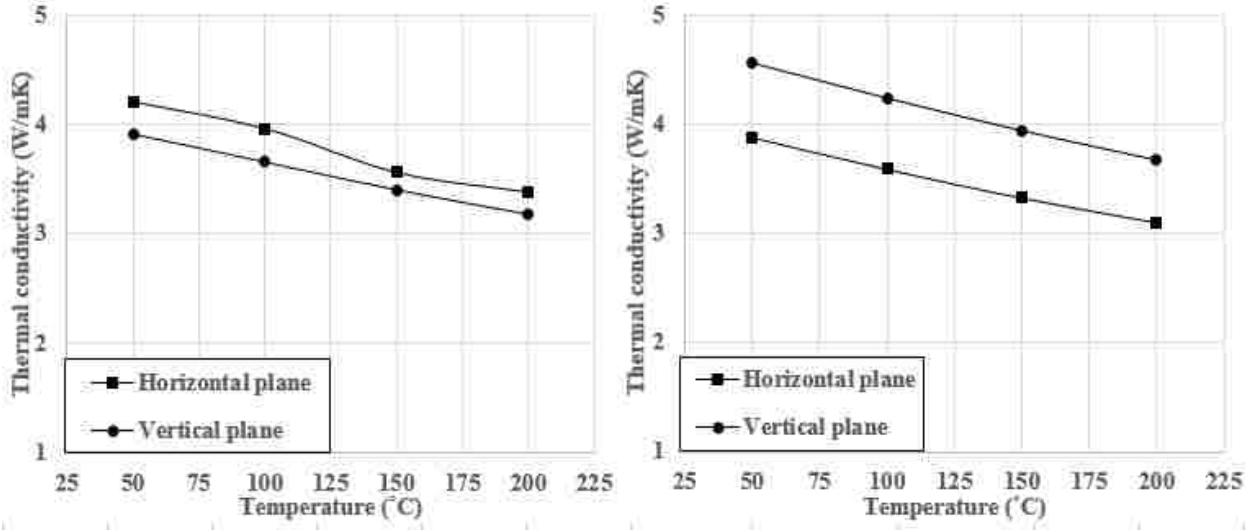

Figure 8 Thermal conductivity of dilated polycrystalline salt samples: WP-DL-200 (left) and WP-DL-250 (right).

3.3 THERMAL PROPERTIES MODELS

3.3.1 Intact salt crystal

Measured thermal conductivity and specific heat of an intact salt crystal were fit as a function of temperature to linear, quadratic, cubic and exponential expressions (Table 4). The measured thermal properties of an intact salt crystal were also compared to other models. Sum of the squared errors (SSE) obtained from the measured and the predicted values are listed in Table 4.

Table 4 Thermal properties of intact salt crystal fitted to empirical equations and compared to other models.

Thermal conductivity equations		**SSE**
Fitting to empirical models	$K_{int} = -7.98x10^{-3}T + 5.876$	0.025
	$K_{int} = 1.374x10^{-5}T^2 - 1.21x10^{-2}T + 6.116$	0.008
	$K_{int} = -1.12x10^{-7}T^3 + 6.414x10^{-5}T^2 - 1.87x10^{-2}T + 6.352$	0.005
	$K_{int} = 5.996e^{-0.002T}$	0.218
Comparison to other models	$K_{int} = 1.2x10^{-1}T^{-2} - 6.11T + 7.01$ [8]	1.210
	$K_{int} = -1.717x10^{-8}T^3 + 3.12x10^{-5}T^2 - 2.1x10^{-2}T + 7.07$ [18]	0.646[(1)]
	$K_{int} = -1.51x10^{-8}T^3 + 2.86x10^{-5}T^2 - 1.838x10^{-2}T + 5.734$ [3]	5.237
	$K_{int} = -2x10^{-7}T^3 + 1x10^{-4}T^2 - 3.17x10^{-2}T + 6.8203$ [11]	6.887
Specific heat equations		**SSE**
Fitting to empirical models	$C_{int} = 2.92x10^{-3}T + 1.9$	0.004
	$C_{int} = -3.43x10^{-7}T^2 + 3.02x10^{-3}T + 1.894$	0.004
	$C_{int} = -6x10^{-8}T^3 + 2.665x10^{-5}T^2 - 5.17x10^{-4}T + 2.02$	0.005
	$C_{int} = 1.929e^{0.0013T}$	0.006
Comparison to other models	$C_{int} = -1.09x10^{-3}T^{-2} + 2.83x10^{-2}T + 2.06x10^{-1}$ [8]	1.048
	$C_{int} = 3.499x10^{-10}T^3 - 8.453x10^{-7}T^2 + 6.43x10^{-4}T + 1.864$ [18]	0.210 [(1)]
	$C_{int} = 0.177T + 855$ [3]	1.010

[(1)]Thermal conductivity and specific heat equations were obtained by fitting the recommended values. T is temperatue in degree Celsius except for [6] is in Kelvin.

3.3.2 Granular salt

Thermal properties of granular salt were fit to the following expressions

$$K_{gs}(T,\phi) = K_{int}(T)f(\phi) \quad (10)$$

$$C_{gs}(T,\phi) = C_{int}(T)g(\phi) \quad (11)$$

With these expressions, the dependence on temperature is accounted for by the term for the thermal property of intact salt. The second term in these expressions is a function of porosity only. Using the linear expressions for thermal conductivity and specific heat given in Table 4 for $K_{int}(T)$ and

$C_{int}(T)$, various forms for the functional dependence on porosity ($f(\phi)$ and $g(\phi)$) were fit to data (Table 5). The data are also compared with other models in Table 5.

Table 5 Thermal properties of granular salt fitted to empirical equations and other models.

Thermal conductivity equations		**SSE**
Fitting to empirical models	$K_{gs} = K_{int}(1 - 2.46\phi)$	5.869
	$K_{gs} = K_{int}(5.08\phi^2 - 3.696\phi + 1)$	4.140
	$K_{gs} = K_{int}(-1.207\phi^3 + 5.556\phi^2 - 3.735\phi + 1)$	4.138
	$K_{gs} = K_{int}(47.64\phi^4 - 29.44\phi^3 + 10.23\phi^2 - 3.89\phi + 1)$	4.111
	$K_{gs} = K_{int}\, e^{-3.73\phi}$	4.168
Comparison to other models	$K_{gs} = K_{int}(1 - 2.7\phi)$ [3]	7.214
	$K_{gs} = K_{int}(-54\phi^4 + 74\phi^3 - 27.2\phi^2 + 0.3\phi + 1)$ [15]	13.360
	$K_{gs} = K_{int}^{1-\phi} K_a^{\phi}$ [14]	10.464
Specific heat equations		**SSE**
Fitting to empirical models	$C_{gs} = C_{int}(1 - 1.7\phi)$	0.655
	$C_{gs} = C_{int}(-2.525\phi^2 - 1.17\phi + 1)$	0.535
	$C_{gs} = C_{int}(-8.305\phi^3 - 0.5\phi^2 - 1.04\phi + 1)$	0.477
	$C_{gs} = C_{int}(-383.77\phi^4 + 221.75\phi^3 - 39.61\phi^2 + 0.43\phi + 1)$	0.372
	$C_{gs} = C_{int}\, e^{-2.107\phi}$	0.850
Comparison to other models	$C_{gs} = C_{int}(1 - \phi)$ [3]	2.257
	$C_{gs} = C_{int}(1 - \phi) + C_a\phi$ [19]	2.259

T is temperatue in degree Celsius and ϕ is porosity.

Chapter 4 DISCUSSION

4.1 POROSITY OF GRANULAR SALT

The similarity of porosities calculated using the porosimeter, which determines connected porosity, and MV method, which estimate the total porosity, indicated the porosity of laboratory-consolidated samples was largely connected. Porosity of sub-samples was mostly greater than the central cores. This suggests the specimens may not have deformed uniformly. Typically the central portion of the core appeared to be smaller than near the top and bottom (Figure 9), which would favor a lower porosity of the central cores compared to the ends where the sub-samples were obtained.

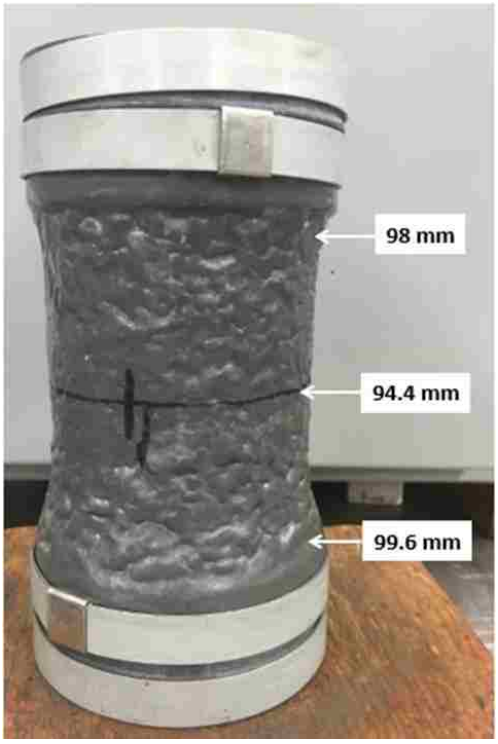

Figure 9 A consolidated specimen with diameters measured at the center and near top and bottom.

4.2 THERMAL PROPERTIES OF INTACT SALT CYSTAL

The thermal properties of intact salt crystal were measured in a temperature range of 50 ˚C to 250 ˚C. The thermal conductivity of the intact salt crystal decreased with increasing temperature, which is consistent with the results of others [2, 3, 7, 8, 9, 10, 11, 18]. The thermal properties of intact salt crystal were fit to various forms of polynomial equations. Both the thermal conductivity and specific heat of an intact salt crystal were well fit as a linear function of temperature. Higher order polynomials provide a slightly better fit but are more likely to significantly deviate from expected trends if used to extrapolate beyond the measured data. Expressing thermal properties as a linear function of temperature is a common form for other geologic minerals [20] and has previously been used for rock salt [3, 21]. For a data set from a larger range of temperatures, a higher order polynomial fit may be more appropriate, such as that given by Urquhart and Bauer [11] for a range from -75 ˚C to 300 ˚C.

Specific heat of an intact salt crystal increased with increasing temperature, which is consistent with results by others [3, 8, 18]. In contrast, Urquhart and Bauer [11] found no clear temperature dependence of specific heat for intact salt crystal. The measured specific heat values were greater than [11] at all the temperatures.

4.3 THERMAL PROPERTIES OF GRANULAR SALT

The observed trend of temperature and porosity dependence of granular salt was consistent with results of others [3, 13] i.e., thermal conductivity decreased with increasing temperature and porosity. The data was well fit with the form of Equations 10 and 11, and various mathematical

forms were used to capture the dependence on porosity (Table 5), quadratic, cubic, and exponential forms performed nearly equally.

Specific heat at lower temperatures was observed to decrease with an increase in porosity. However, at higher temperatures, porosity dependence was not apparent (Figure 7). Bechthold et al. [3] reported specific heat decreased with an increase in porosity at room temperature. Bauer and Urquhart [13] reported little porosity dependence of specific heat.

Using the mixing law, 1% added water would increase the thermal conductivity by more than 5% which is within the resolution of the measurement technique. However, the samples consolidated with 1% added water do not result in systematically greater thermal conductivities compared to samples compacted without added water (Table 3 and Figure 7). The added water was likely involved in pressure solutioning at grain contacts [6], which involves the dissolution and precipitation of salt at grain boundary contacts. This mechanism may produce isolated fluid inclusions along remnant grain boundaries and not a continuous water phase within a pore network; isolated pores and fluid inclusions may not significantly impact the effective thermal properties for the entire mass. Further, at the elevated temperatures during the consolidation test, some of the added water may have evaporated and removed from the vented samples.

There were only two tests on AI salt, both samples were consolidated at 250 ˚C. Compared to the WIPP salt, the thermal conductivity of AI salt is greater at comparable porosities and at higher temperatures (Table 3 and Figure 7). Differences in thermal conductivity may be a result of differing amounts of impurities [20] in the two types of salt; WIPP salt has between 1 and 5%

water insoluble impurities [13, 22] whereas the AI salt has roughly 0.7% of water insoluble impurities [2]. At comparable porosities, there is not much difference in the specific heat of WIPP and AI salt.

Thermal conductivities measured in this study were generally greater than those measured by Bauer and Urquhart [13] at all temperatures (Figure 10) in spite of the fact that the majority of the granular salt stock material was from the same location (WIPP) and the same measurement method was used.

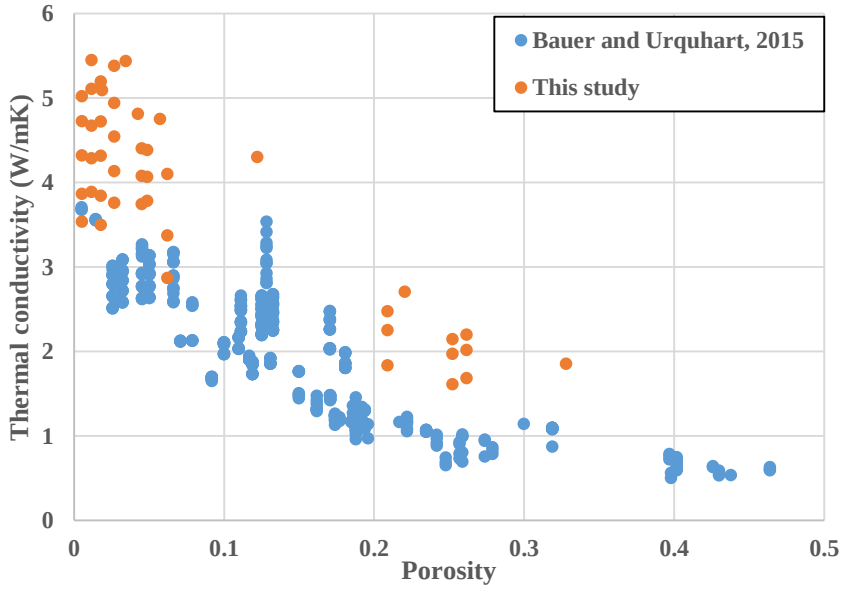

Figure 10 Thermal conductivity of consolidated salt compared with pellet pressed salt [11] in a temperature range of 50-250 ˚C.

The difference between the results given here and those of Bauer and Urquhart [13] were likely due to the nature of the porosity developed during the different sample preparation methods. Bauer and Urquhart [13] pressed granular salt in pellets at room temperature whereas this study involved hydrostatic consolidation of granular salt at elevated temperatures and pressures. Photomicrographs of hydrostatically consolidated and pressed samples with similar porosities are

shown in Figure 12. The hydrostatically consolidated sample has fully sutured or fused grain boundaries and a near absence of microcracks. The consolidation involved gradual loading and unloading under elevated temperatures and substantial hydrostatic stresses. These conditions are expected to promote plastic deformation during consolidation and prevent cracking during unloading (depressurization). Grain boundaries coalesced by plastic deformation at molecular scale. The presence of water favors consolidation [6], whether as added or mobilized from the salt at elevated temperatures [16]. In contrast, the pressed samples experienced rapid loading and unloading at ambient temperature and pressure conditions. These conditions resulted in cleavage cracking and microfracturing at grain boundaries. At high porosities cracks formed at grain contacts during mechanical consolidation. As the pressing progressed, most of the porosity subsequently closed. Upon unloading, however, the stored strain energy within the grains in structures relieved by the formation of cracks along grain boundaries and through grains along cleavage planes, made apparent by the presence of stained epoxy. Therefore, the hydrostatically consolidated salt consists of tubular pores (Figure 11), whereas the axially pressed sample includes significant crack porosity (Figure 11) around or through the crystals. Sensible heat transferred largely by conduction finds a preferred path through the solid matrix of salt, which is more than 100 times more conductive than the air [23]. Hence heat flow is expected to circumvent a tubular pore network, whereas it must cross open grain boundaries and microcracks in samples with crack porosity. Heat flow is inhibited more in the latter case and results in a lower thermal conductivity at a comparable density.

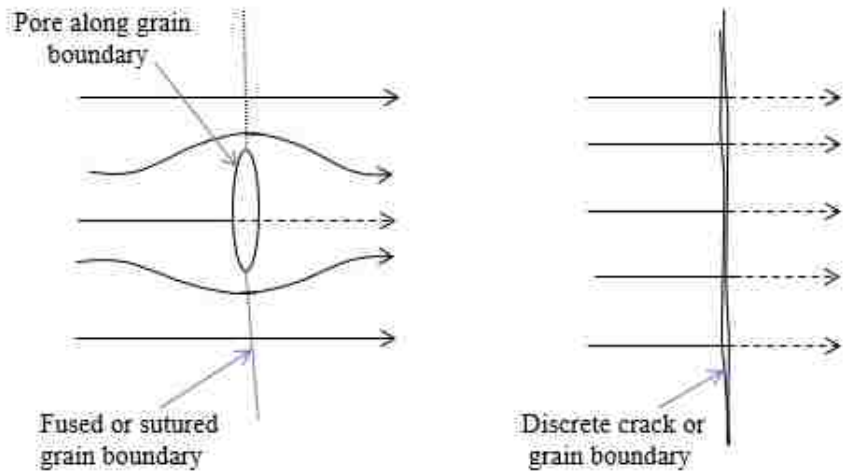

Figure 11 Schematic of the influence of nature of porosity developed from consolidation (left) and pressing (right) on heat flow at comparable porosities.

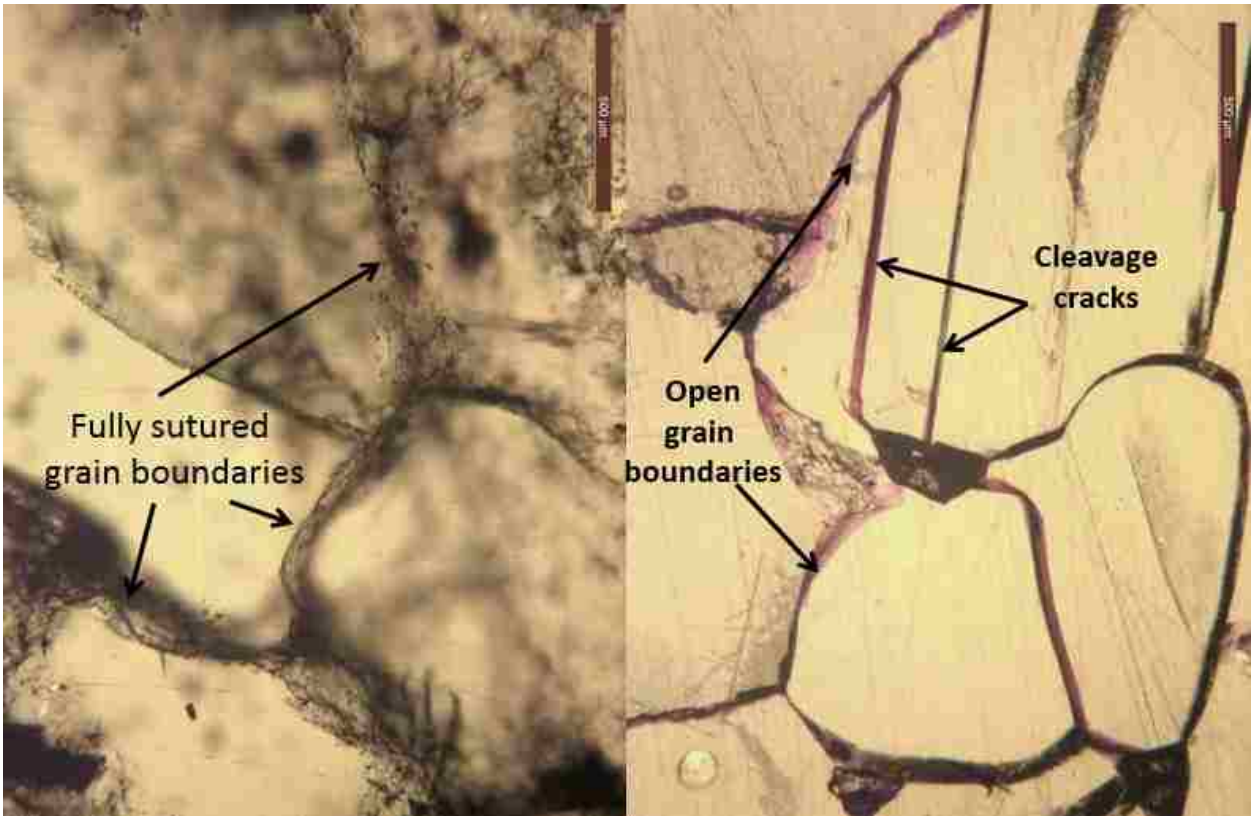

Figure 12 Consolidated salt (left) and axially pressed salt (right) at comparable porosities of less than 0.02.

4.4 DILATED SALT

The dilated salt had a lower thermal conductivity compared to consolidated salt at a comparable porosity (Figure 13). Thermal conductivity measured along the horizontal plane was greater than that measured along vertical in one sample, but an opposite trend was observed in the other. The porosity of dilated salt consists of a network of high aspect ratio (width to height) along grain boundaries, whereas in consolidating granular salt, the porosity evolves toward a tubular network [5]. Heat flow will likely be more inhibited by the pervasive crack network as suggested by Bauer and Urquhart [11].

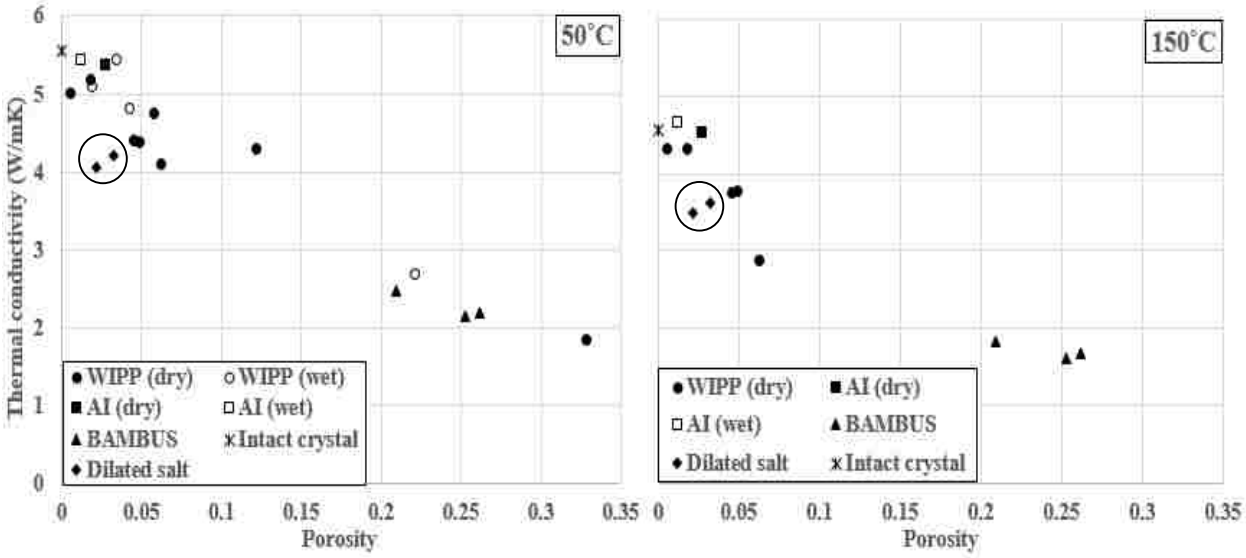

Figure 13 Thermal conductivity of dilated salt (encircled) compared with thermal conductivity of other salt types.

Chapter 5 CONCLUSIONS

Thermal properties and porosity tests measurements were conducted on various types of salt at various temperatures and porosities. More than 400 thermal properties measurements were made using a transient plane source method and 65 porosity measurements were made with a porosimeter. In addition to this, some porosity measurements were made using a permeameter configured as a gas expansion porosimeter. Experimental data were fit to various empirical equations and were compared to models derived from studies of others.

The similarity of the porosities derived from porosimeter, which determined connected porosity, and MV method, which estimated the total porosity, indicates the porosity of laboratory-consolidated samples is largely connected. Porosity of sub-samples obtained from the ends of the cores was mostly greater than that from the central portion of the cores. This result suggests that the specimens did not deform uniformly.

Thermal conductivity of an intact salt crystal showed strong dependence with temperature i.e., thermal conductivity decreased with increase in temperature. These data were well fit as a linear function of temperature which is a common form for other geologic minerals. Thermal conductivity of granular salt was dependent on temperature and porosity; thermal conductivity decreased with an increase in temperature and porosity. Thermal conductivity of granular salt was expressed as a function of the thermal conductivity of intact salt and the porosity, as $K_{gs}(T,\phi) = K_{int}(T)f(\phi)$. Quadratic, cubic, quartic and exponential forms for $f(\phi)$ were found to perform nearly equally well in capturing the dependence on porosity.

The majority of the thermal and porosity measurements were made on samples subjected to hydrostatic creep consolidation with stresses and temperatures relevant to potential repository conditions. Creep consolidation tests generated a pore structure consistent with the deformation mechanisms expected to be operative at repository conditions, particularly with regard to the nature of the grain boundaries. We therefore expect these measurements to be directly relevant to the response of granular salt in a repository application.

Thermal conductivities measured in this study were generally greater than that those measured by Bauer and Urquhart [13] at all temperatures in spite the fact that the granular salt stock material was largely from the same location (WIPP) and the same measurement method was used. Bauer and Urquhart [13] pressed granular salt in pellets at room temperature whereas this study involved hydrostatic consolidation of granular salt at elevated temperatures and pressures. Photomicrographs of hydrostatically consolidated and pressed samples with the same porosities showed that the hydrostatically consolidated sample had fully sutured grain boundaries and a near absence of microcracks. In contrast, the pressed samples had intense cleavage cracks and microfracturing at grain boundaries.

Thermal conductivity of dilated salt was determined to be lower than the consolidated salt at comparable porosities. The pervasive crack network along grain boundaries in dilated salt is hypothesized to limit heat flow, and result in a lower thermal conductivity compared to hydrostatically consolidated salt.

Specific heat of intact salt crystal was shown to increase with an increase in temperature, which was fit with a linear function. Specific heat of granular salt at lower temperatures was shown to decrease with an increase in porosity. At higher temperatures porosity dependence was not apparent. The specific heat of granular salt was expressed as a function of the specific heat of intact salt and measured porosity, $C_{gs}(T,\phi) = C_{int}(T)g(\phi)$. The linear form for $g(\phi)$ was determined to adequately describe the dependence on porosity.

REFERENCES

1. National Research Council. Disposition of High Level Waste and Spent Nuclear Fuel. Committee on Disposition of High Level Radioactive Waste through Geological Isolation. Board of Radioactive Waste Management. ISBN 0-309-56764-5. 2001:22-26.
2. Durham WB, Abey AE. Thermal Properties of Avery Island Salt to 573 K and 50-MPa Confining Pressure. Livermore (CA): Lawrence Livermore National Laboratory.1981; UCRL-53128.
3. Bechthold W, Rothfuchs T, Poley A, Ghoreychi M, Heusermann S, Gens A, Olivella S. Backfilling and sealing of underground repositories for radioactive waste in salt (Bambus Project): Final Report. EUR 19124 EN. European Commission, Brussels, 1999.
4. Martin BL, Rutqvist J, Birkholzer JT. Long-term modeling of the thermal-hydraulic-mechanical response of a generic salt repository for heat-generating nuclear waste. *Eng Geol*. 2015;193:198-211. doi:10.1016/j.enggeo.2015.04.014.
5. Hansen F, Popp T, Wieczorek K, Stuhrenberg D. Granular Salt Summary: Reconsolidation Principles and Applications. SAND2014-16141R. Albuquerque (NM): Sandia National Laboratories; 2014.
6. Stormont JC, Finley RE. Sealing Boreholes in Rock Salt. In: Fuenkajorn K, Daemen JJK, eds. Sealing of Boreholes and Underground Excavations in Rock. doi:10.1007/978-94-009-1505-3. Chapman and Hall.1996:204-209.
7. Birch F, Clark H. The thermal conductivity of rock and its dependence upon temperature and composition: Part I. Am J Sci. 1940;238:529-558.
8. Smith D. Report no.: Y/DA-7013. Thermal conductivity of halite using a pulsed laser. Oak Ridge (TN): Oak Ridge Y- Plant; 1976 39 pp. Contract no.: W- 7405-eng-26. Supported by the US Energy Research and Development Administration.
9. Acton U. Thermal Conductivity of S.E. New Mexico Rocksalt and Anhydrites. In: International Conference on Thermal Conductivity, 15th. Ottawa; 1977:263-276.
10. Sweet JN, McCreight JE. Thermal conductivity of rocksalt and other geologic materials from the site of the proposed waste isolation pilot plant. SAND79-1134. Albuquerque (NM): Sandia National Laboratories; 1979.

11. Urquhart A, Bauer S. Experimental determination of single-crystal halite thermal conductivity, diffusivity and specific heat from -75°C to 300°C. Int J Rock Mech Min Sci. 2015;78:350-352.doi:10.1016/j.ijrmms.2015.04.007.
12. van den Broek WMGT. Impurities in rock-salt: consequences for the temperature increases at the disposal of high-level nuclear waste. PB-83-102087. Technische Hogeschool Delft, Netherlands, 1982.
13. Bauer S, Urquhart A. Thermal and physical properties of reconsolidated crushed rock salt as a function of porosity and temperature. Acta Geotech. 2015. doi:10.1007/s11440-015-0414-8.
14. Macaulay DB, Bouazza A, Wang B, Singh RM. Evaluation of thermal conductivity of models. Can. Geotech. J. 52:1892-1900;2015.
15. Bechthold W, Smailos E, Heusermann S, Bollingerfehr W, Bazargan Sabet B, Rothfuchs T, Kamlot P, Grupa J, Olivella S, Hansen F. Backfilling and sealing of underground repositories for radioactive waste in salt (Bambus II Project): Final Report. EUR 20621 EN. European Commission, Luxembourg, 2004.
16. Broome ST, Bauer SJ, Hansen FD. Reconsolidation of Crushed Salt to 250°C Under Hydrostatic and Shear Stress Conditions. In: 48th US Rock Mechanics/Geomechanics Symposium. Minneapolis; 2014.
17. Coberly CJ, Stevens AB. Development of Hydrogen Porosimeter. Society of Petroleum Engineers. SPE-933261-G; 1933: 261-269.
18. Yang JM. Thermophysical Properties. In: Gevantman LH, eds. Physical Properties Data for Rock Salt. Monograph 167. National Buerau of Standards, Washington. 1981:206-212.
19. Jury WA, Horton R. Soil Physics. 6th ed. Hoboken, NJ: Wiley; 2004:180-182.
20. Clauser C, Huenges E. Thermal Conductivity of Rocks and Minerals. In: A Handbook of Physical Constants. AGU Reference Shelf 3. American Geophysical Union. 1995: 105-125.
21. Clark Jr SP. Heat conductivity in the mantle. In: Hart PJ, eds. The earth's crust and upper mantle. Amer. Geophys. Union. Geophysical Monograph 13. Washington, 1969:622-626.
22. Stein CL. Mineralogy in the waste isolation pilot plant (WIPP) facility stratigraphic horizon. SAND85-0321. Albuquerque (NM): Sandia National Laboratories; 1985 32 pp.
23. Joy AF. Thermal conductivity of insulation containing moisture. ASTM International. 1957:65-67.

APPENDIX

A.1 Water loss experiment

A.1.1 Methodology

Four aluminum trays were marked with sample names and measured for the individual empty mass. Two samples each of AI and WIPP salt, grain size less than 9.5mm, were placed in a thin layer on the trays and measured for mass at room temperature. The samples were placed in oven with a starting temperature of 50 ˚C as shown in Figure A1. Once no more water loss was observed at a particular temperature in two consecutive readings, the oven temperature was raised by 50 ˚C. The highest temperature for the test was 250 ˚C.

Figure A1 Granular salt placed inside the oven (left) and a digital weighing machine measuring the mass of salt.

A digital balance with a precision of 0.01 gram was used for measuring the mass. The weighing machine (Figure A1) was placed in close vicinity of the oven to shorten the measurement time. Samples were measured immediately after removing from the oven each time, and replaced inside the oven for another test scheduled approximately after 24 hours. 82.44 grams of WP2 salt was lost during accidental spill. The lost mass of salt was determined by subtracting the left over mass from last known mass.

A.1.2 Results

The percent of water loss at different temperatures and the cumulative water loss are summarized in Table A1. The loss in mass of samples is given in Figures A2 and A3. Results show that water loss from the WIPP salt is greater than that from the AI salt in a time period of 70 days. A slight gain in mass was observed at some temperatures, which was likely a result of change in atmospheric humidity, sensitivity of machine to circulating air and vibrations from other machines.

Table A1 Summary of water loss experiment.

Sample	Water loss at 50 ˚C in 20 days (%)	Water loss at 100 ˚C in 21 days (%)	Water loss at 150 ˚C in 11 days (%)	Water loss at 200 ˚C in 7 days (%)	Water loss at 250 ˚C in 11 days (%)	Cumulative water loss in 70 days (%)
AI1	0.013	0.082	0.038	0.054	0.038	0.224
AI2	0.009	0.076	0.049	0.03	0.046	0.209
WP1	0.066	0.138	0.05	0.075	0.041	0.369
WP2	0.04	0.045	0.094	0.074	0.074	0.34

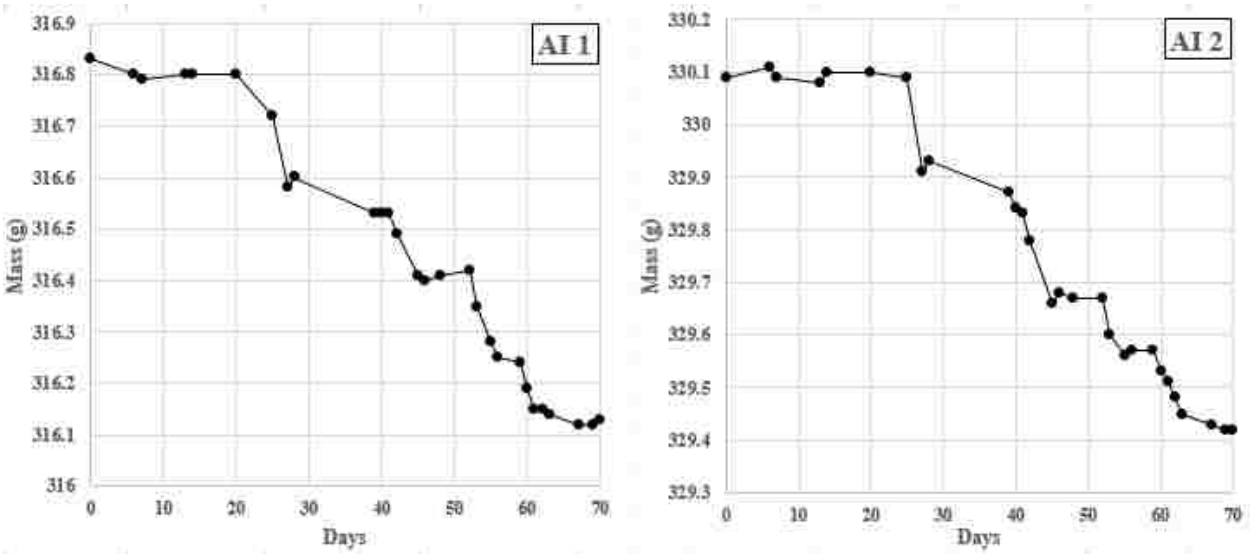

Figure A2 Water loss from AI salt samples in 70 days.

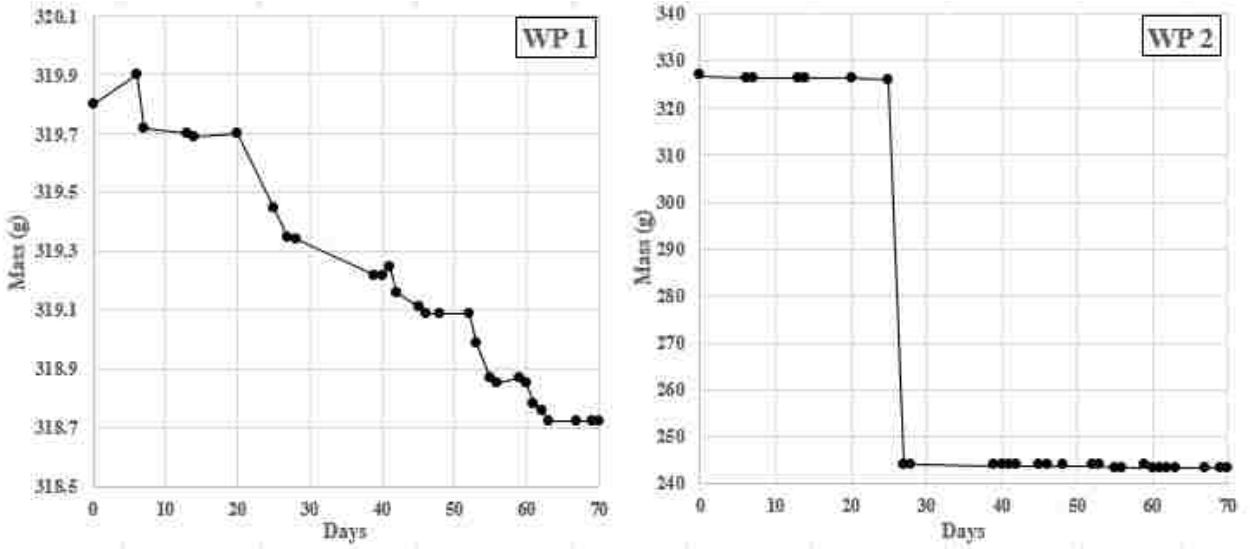

Figure A3 Water loss from WIPP salt samples in 70 days.